IYC'09 2nd International Youth Conference on Energetics 2009

Development of a 3D Nodal Solver with the Migration Mode Method

Daniele Tomatis

***Abstract* – In the present work, a 3D nodal solver for neutronic calculation is developed with the Migration Mode Method in diffusion theory. The nodal approach acts as a correction to a finite difference scheme applied on a coarse Cartesian mesh. Critical steady state tests on full cores are shown with few mode fast calculations. Similar results for an equivalent multigroup model are compared trying to keep the same number of unknowns and constraints. Improvements of the method are discussed with reference to fine and detailed multigroup solutions. Features like flux discontinuity factors needs to be re-defined with this method, as well as extrapolated lengths for zero incoming current boundary conditions.**

***Index Terms* — Criticality, Diffusion, Fission reactors, Numerical analysis, Neutrons, Spectral analysis.**

I. Nomenclature

MMM – Migration Mode Method;
MGM – Multi-Group Method;
MEM – Modal Expansion Method;
FEM – Finite Element Method;
SSM – Spectral Synthesis Method.

II. Introduction

THE standard procedure for the energy treatment in nuclear chain reactors is based on the application of the multigroup (MGM) theory. It consists of a subdivision of the energy axis imposing constant solutions herein. Detailed calculations with very fine MGM neutron transport theory determine reference spectrum distributions in reflected fuel assemblies, which are then used to collapse and homogenize material cross sections in broader sets [12]. These data are then employed for further problems, solving simpler models like neutron diffusion, to compute quickly the neutron flux distribution, and consequently, the thermal power generated by fission, in the full core. Moving to broader cross section sets in energy is defined always saving reaction rates over specific non-overlapping energy ranges, thus keeping the same reactivity in the system. But this process drops punctual information in energy of the neutron spectrum for the nodes of the modeled full core. Solutions to reduce the loss of information in the collapsing have been recently introduced. Particular attention deserves the generalization of the MGM through in-group expansion models [9]. Also some FEM-like approaches denote the strong interest in the energy topic [13]. But each MGM hides the intrinsic assumption of a synthesis using the original detailed reference neutron spectrum of the fuel assembly, while collapsing still in infinite media [14]. This process postulates material homogeneity and large dimensions in the core indeed. The former point cannot be assured anymore with the common MO_X fuel load strategy. To model more accurately neutron systems, a step back in the energy treatment at full core level must be done, returning to SSMs [6]. The MMM is another SSM, which improves the coarse spectral description done by the MGM. Here, the energy dependence is studied employing different spectral migration modes, which may analyze the problem under different physical aspects. These modes were studied since the beginning of the Reactor Theory to interpret nuclear experiment and find effective cross sections [1, 12]. First energy syntheses applied to complex systems appeared with the MEM already in the 60's [3]. The main aim for MEM was modeling efficiently fast reactor, for which only many group MGM calculations, computationally expensive, could give accurate solutions. The MMM expands the neutron flux with a superposition of functions in energy, called the migration modes [7]. This particular SSM presents similar aspects with the MEM, but its application takes here particular attention to thermal light water reactors (LWRs).

III. The Migration Mode Method

SSMs have been largely applied to solve Partial Differential Equations with rather success in obtaining good computational results. Such methods approximate the solution with sums of products given by known trial functions and their correspondent contributions, which are the new unknown coefficients. Trial functions, which carry the synthesis, can be defined over the whole phase space, while their coefficients are limited to particular subspaces, thus solving simpler weak problems. This synthesis approximation introduces more

This work was supported in part by AREVA NP under a scholarship grant.
D. Tomatis is a PhD candidate at Politecnico di Torino, Corso Duca degli Abruzzi 24, 10129 Torino - Italy (e-mail: daniele.tomatis@polito.it).

unknowns into the governing equation needing further closures, which come projecting the original problem over special test functions. These last ones allow achieving peculiar properties of the reference problem [2]. In MMM weighting by generalized importance functions turns out as a profitable choice [14]. The MMM considers trial functions defined uniquely over the whole energy range choosing physical migration modes of neutrons. After having selected a set of M migration modes Q_m, the MMM adopts the following assumption for the neutron angular flux $\varphi(\mathbf{y}, E)$:

$$\varphi(\mathbf{y},E)=\sum_{i=1}^{M} a_m(\mathbf{y})Q_m(\mathbf{y},E), \qquad (1)$$

being $\mathbf{y} = \{\mathbf{r}, \mathbf{\Omega}, t\}$. Briefly, the neutron angular flux is a probability density function counting neutrons at the position $\mathbf{r}$ in $d\mathbf{r}$ flying with direction $\mathbf{\Omega}$ around $d\mathbf{\Omega}$ of energy E in dE and at the time t. The order M of expansion fixes the number of new unknown a_m functions and the pursued computational target. Looking for syntheses in energy of infinite media, a stronger approximation is advanced in MMM: $Q_m(\mathbf{y}, E) \rightarrow Q_m(E)$. This imposes a separability condition of variables too, whose consistency needs always to be verified. The energy distribution of neutrons shows three major distinct behaviors, which are especially evident into thermal reactors regardless of the kind of fuel. Their shape is slightly modified all around the core by small drifts or normalization scaling. This fact suggests syntheses by these same modes. The first is a Maxwellian distribution Q_M describing neutrons at thermal equilibrium with atoms of the surrounding medium. This mode goes like $E/E_N{}^2 \exp[-E / E_N]$, where E_N is the modal value of the distribution, i.e. the most probable one, proportional to the neutron temperature T_N through the Boltzmann's constant k. The second mode Q_{SD} shapes the neutron slowing down with a 1 / E –like distribution. Due to all hard self-shielding effects of resonances, this mode entails a big effort to reproduce reliably the spectrum. Finally, the distribution χ of fission emitted neutrons takes into account fast energies too. χ looks like $E\exp[-\alpha E]$, with $\alpha > 0$.

IV. MMM Diffusion Model

This section presents a diffusion model with the Migration Mode Method to describe the population of neutrons. As well known, diffusion theory can be derived by P_1 transport with possible isotropic external sources and stationary conditions. By the standard definition of the scalar flux ϕ and current $\mathbf{J}$, the angular flux φ in P_1 can be formulated as:

$$\varphi(\mathbf{r},E,\mathbf{\Omega})=\frac{1}{4\pi}\left[\phi(\mathbf{r},E)+3\mathbf{\Omega}\cdot\mathbf{J}(\mathbf{r},E)\right],$$
$$\phi(\mathbf{r},E)=\oint_{4\pi}\varphi\, d\mathbf{\Omega},\ \ \mathbf{J}(\mathbf{r},E)=\oint_{4\pi}\mathbf{\Omega}\varphi\, d\mathbf{\Omega}\ . \qquad (2)$$

Neutron balance equation, closed by the Fick's law, leads to the following diffusion model for neutrons:

$$\begin{cases}\nabla_{\mathbf{r}}\cdot\mathbf{J}(\mathbf{r},E)+\Sigma_t(\mathbf{r},E)\phi(\mathbf{r},E)=S_{ext}+\\ \int_0^{\infty}\Sigma_s(\mathbf{r},E'\rightarrow E)\phi(\mathbf{r},E')\,dE'\\ +\chi(\mathbf{r},E)\int_0^{\infty}\nu\Sigma_f(\mathbf{r},E')\phi(\mathbf{r},E')\,dE',\\ \mathbf{J}(\mathbf{r},E)=-D(\mathbf{r},E)\nabla_{\mathbf{r}}\phi(\mathbf{r},E),\end{cases} \qquad (3)$$

where Σ_t, Σ_s, Σ_f, χ, ν and D are respectively, the macroscopic total, scattering, fission cross sections, the emission probability density from fission, the average number of neutrons produced by fission and the diffusion coefficient. For practical reason ν is included in the fission cross section. S_{ext} takes into account external neutron sources. With the mentioned assumptions, P_1 verify Fick's law, giving $D = 1 / 3\ \Sigma_{tr}$, $\Sigma_{tr} = \Sigma_t - \mu_{av}\ \Sigma_s$, being μ_{av} the average scattering angle. For the energy dependence, the previous statement still needs the next approximation [12]:

$$\int_0^{\infty}\Sigma_s(\mathbf{r},E'\rightarrow E)\mathbf{J}(\mathbf{r},E')\,dE'\approx$$
$$\mathbf{J}(\mathbf{r},E)\int_0^{\infty}\Sigma_s(\mathbf{r},E'\rightarrow E)\,dE'.$$

Substituting Fick's law for neutron current $\mathbf{J}$ in the balance equation, the solution flux is demanded to be $C^2(\mathbb{R})$; this brings to a further constraint, not requested in transport.

The MGM integrates the system of Eq.s (3) in a set of G energy ranges, as using fictitious unitary test functions and picking the only contribute of neutrons localized in certain energy windows [14]. The flux becomes then a step-wise constant function in energy and new material constants must be defined to keep unaltered reaction rates. The MGM diffusion equations are:

$$\begin{cases}\nabla_{\mathbf{r}}\cdot\mathbf{J}_g(\mathbf{r})+\Sigma_{t,g}(\mathbf{r})\phi_g(\mathbf{r})=S_g(\mathbf{r})+\\ \sum_{g'=1}^{G}\left[\Sigma_{s,g'\rightarrow g}+\chi_g\nu\Sigma_{f,g'}\right](\mathbf{r})\phi_{g'}(\mathbf{r}),\\ \mathbf{J}_g(\mathbf{r})=-D_g(\mathbf{r})\nabla_{\mathbf{r}}\phi_g(\mathbf{r});\ \ g=1,\ldots,G.\end{cases} \qquad (4)$$

where, $\phi_g=\int_{E_{g+1}}^{E_g}\phi(\mathbf{r},E)\,dE$, $\chi_g=\int_{E_{g+1}}^{E_g}\chi(\mathbf{r},E)\,dE$,

$$\Sigma_{p,g}=\frac{1}{\phi_g}\int_{E_{g+1}}^{E_g}\Sigma_p(\mathbf{r},E)\phi(\mathbf{r},E)\,dE,$$

$$\Sigma_{s,g'\to g} = \frac{1}{\phi_{g'}} \int_{E_{g+1}}^{E_g} \left[\int_{E_{g'+1}}^{E_{g'}} \Sigma_s(\mathbf{r}, E' \to E)\, \phi(\mathbf{r}, E')\, dE' \right] dE \,.$$

Here, the subscript p refers to a general cross section. S_g is evaluated similarly to ϕ_g. Collapsing the diffusion coefficient is not a simple task, because it demands a weighting with the spatial gradient of the flux. In case of homogeneous material it simplifies to a Σ_p object.

Introducing Eq. (1) into Eq.s (3) and weighting with M continuous test functions $U_l(E)$, the MMM diffusion model follows:

$$\begin{cases} \nabla_{\mathbf{r}} \cdot \mathbf{J}_l(\mathbf{r}) = S_l(\mathbf{r}) + \\ \sum_{m=1}^{M} \left[\Sigma_{s,lm} + \chi_l \nu\Sigma_{f,m} - \Sigma_{t,lm} \right](\mathbf{r})\, a_m(\mathbf{r}), \\ \mathbf{J}_l(\mathbf{r}) = \int_0^\infty U_l(E)\, \mathbf{J}(\mathbf{r}, E)\, dE = \\ -\sum_{m=1}^{M} D_{lm}(\mathbf{r}) \nabla_{\mathbf{r}} a_m(\mathbf{r}), \; l = 0, ..., M-1. \end{cases} \tag{5}$$

where, explicitly,

$$D_{lm} = \int_0^\infty dE\, U_l(E)\, D(\mathbf{r}, E)\, Q_m(E),$$

$$\Sigma_{a,lm} = \int_0^\infty dE\, U_l(E)\, \Sigma_a(\mathbf{r}, E)\, Q_m(E),$$

$$\Sigma_{r,lm} = \int_0^\infty dE\, U_l(E)\, Q_m(E) \int_0^\infty dE' \Sigma_s(\mathbf{r}, E \to E'),$$

$$\Sigma_{s,lm} = \int_0^\infty dE\, U_l(E) \int_0^\infty dE' \Sigma_s(\mathbf{r}, E' \to E)\, Q_m(E'),$$

$$\chi_l = \int_0^\infty dE\, U_l(E)\, \chi(\mathbf{r}, E),$$

$$\nu\Sigma_{f,m} = \int_0^\infty dE\, \nu\Sigma_f(\mathbf{r}, E)\, Q_m(E).$$

It follows that $\Sigma_{t,lm} = \Sigma_{a,lm} + \Sigma_{r,lm}$ and S_l is determined as χ_l. MMM needs a new treatment for cross sections. The choice of the migration modes in the MMM is much less problem dependent than in the MGM with a reference spectrum. To take into account the synthesis error and achieve the same integral parameter k_{eff} in a critical calculation, an equivalent factor f_S is needed [7]. Grouping MMM coefficients of Eq.s (5) under operator forms, the eigenvalue problem for f_S states:

$$\left[\hat{A} + \hat{R} - \frac{1}{k_{eff}} \hat{F} \right] \cdot \mathbf{a} = f_S \hat{S} \cdot \mathbf{a}\,, \; \mathbf{a} = |a_m\rangle\,, \tag{6}$$

where $\hat{A}$, $\hat{R}$, $\hat{F}$ and $\hat{S}$ are respectively the absorption, the removal by scattering events, the fission neutron production and the scattering transfer operators. The physical acceptable f_S requires the synthesized spectra to be positive everywhere. Using the classical adjoint flux, relative to a null adjoint external source, f_S is identically unitary and then the well-known eigenvalue problem for k_{eff} is found again. In core applications, f_S is included directly in the scattering operator.

Many groups MGM cross section tables, referred to a homogenized fuel assembly with reflected boundary conditions, are processed by FORTRAN90 modules to execute all the quadratures needed for MMM cross sections of Eq.s (5). This information, stored as fine step-wise constant functions, puts right to the fact of not having available nuclear libraries of material data.

V. Numerical Solving Method

A. First Level Solver on Coarse Mesh

To solve Eq.s (4), or (5), the geometrical space is discretized in a connected coarse Cartesian orthogonal mesh, upon which a Finite Volume (FV) approach saves the neutron balance in each prismatic k-th sub-element, called node. Integrating over the volume of the k-th node and dividing for it allows applying the divergence theorem for the streaming term of the current, having its surface integral:

$$\begin{aligned} &\frac{1}{V^k} \iint_{S^k} \mathbf{J}(\mathbf{r}, E) \cdot \hat{\mathbf{n}}\, dA + \Sigma_t^k(E)\, \phi^k(E) = \\ &\int_0^\infty \Sigma_s^k(E' \to E)\, \phi^k(E')\, dE' \\ &+ \frac{\chi^k(E)}{k_{eff}} \int_0^\infty \nu\Sigma_f^k(E')\, \phi^k(E')\, dE'; \\ &\frac{1}{V^k} \iint_{S^k} \mathbf{J} \cdot \hat{\mathbf{n}}\, dA = \sum_{i=x,y,z} \frac{J_i^{k+}(E) - J_i^{k-}(E)}{\Delta i^k}. \end{aligned} \tag{7}$$

The superscript k means volume averaged, i.e. as:

$$\phi^k(E) = \frac{1}{V^k} \iiint_{V^k} \phi(\mathbf{r}, E)\, d\mathbf{r}\,,$$

where "+" and "-" indicate positive and negative faces of the k-th node. Material coefficients are considered constant over the k-th node. This technique keeps a second order discretization error. The combination of a Nodal Expansion Method (NEM), played to correct neutron currents at node interfaces, highly increases the accuracy maintaining a coarse mesh, thus saving computation time. For critical problems, the solution of the eigenvalue problem for k_{eff}, with its associated eigenfunction, the fundamental mode of the neutron distribution, is searched with the common Power Iteration Method (PIM). This loops at the level of outer iterations for

new inner source computation by fission, then filtering the fundamental mode. The powerful Wielandt's acceleration boosts the convergence of the solution, decreasing the spectral ratio of the first two eigenvalues of the problem by an eigenvalue shift. Its combination with the power method is here preferred to more modern methods, as Krilov subspace iterations.

Diffusing currents are approximated with a second order finite difference of the kind:

$$J_i^{k\pm}(E) \cong \mp D_i^{k\pm}(E)\frac{\phi_i^{k\pm1}(E)-\phi_i^{k}(E)}{(\Delta i^{k\pm1}+\Delta i^{k})/2}, \qquad (8)$$

where $i = \{x, y, z\}$. Diffusion coefficients evaluated at boundaries are volume averaged at first order:

$$D_i^{k+}(E) \cong \frac{D_i^{k+1}(E)\Delta i^{k+1}+D_i^{k}(E)\Delta i^{k}}{\Delta i^{k+1}+\Delta i^{k}} \qquad (9)$$

and, for the continuity, $D_i^{k+1,-} = D_i^{k+}$. In case of MGM, the i-th component of the neutron current for the g-th group, at the interface ± of the k-th node, $J_{i,g}^{k\pm}$ follows directly from Eq. (8), simply adding the g-th subscript according to Eq.s (4). While the MMM writes the l-th weighed current $J_{i,l}^{k\pm}$ as:

$$\int_0^\infty U_l(E)J_i^{k\pm}(E)dE = J_{i,l}^{k\pm} = \sum_{m=1}^{M} J_{i,lm}^{k\pm} \cong \mp\sum_{m=1}^{M} D_{i,lm}^{k\pm}\frac{a_m^{k\pm1}-a_m^{k}}{(\Delta i^{k\pm1}+\Delta i^{k})/2}. \qquad (10)$$

In Eq. (10) it is possible to identify the l-th weighed m-th modal current $J_{i,lm}^{k\pm}$. Approximating currents with finite differences together with a coarse mesh moves the FV towards the term Coarse Finite Difference Method (CFDM). Substituting these currents in the proper form of Eq. (7) yields a linear system, numerically solvable for unknown g-th fluxes or m-th mode coefficients. Representing again the model through operators, the total removal operator $\hat{L}$, given by the sum of $\hat{A}$ and $\hat{R}$ (see Eq. (6)), assumes a band matrix form, denoted now as **L**, dominated by main diagonal elements. Analyzing **L** under the MGM and the MMM it appears clearly that the last one shows a reduced degree of sparsity. The algebraic solution is determined with the Jacobi method for which the denser MMM **L** does not need different treatments compared to the MGM. Inside the PIM, mathematical inhomogeneous problems are solved iteratively until achieving converged fission reaction rates. Here, sources keep the same matrix structure either for the MMM or the MGM. Jacobi method splits **L** in a sum of a diagonal-like matrix **D**, a lower triangular matrix **N** and an upper triangular matrix **M**. In **D** it is collected all the energy information of the single node problem where the diffusion coefficient acts as part of a fictitious extra removal cross section. While **N** and **M** keep respectively the correspondent coefficients of $^{(-)}$ left nodes and $^{(+)}$ right nodes per each coordinate. Because of the chosen second order numerical scheme for the streaming, diffusion couples only close nodes. In the built spatial grid, this implies that, with a representation of the nodes as in a red-black checkerboard scheme (CBS), mainly ordered following the x direction and nested sequentially with y and z ones, red nodes are linked only with black ones and vice versa (Fig. 1).

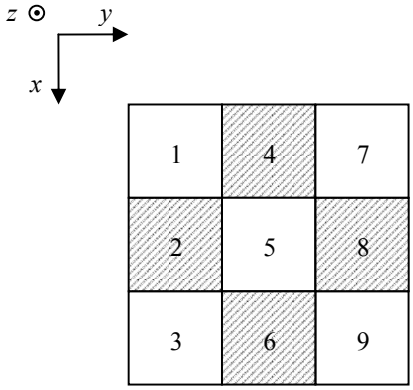

Fig. 1. CBS representation for a simple 2-D spatial domain.

The CBS allows separated computation of black b and red r nodes. As a numerical method, it was mainly conceived to save storage memory, but this effect is of less importance. The strong effectiveness of the CBS is to increase convergence rate of the stand alone slow Jacobi method. At the s-th step of the n-th outer iteration, $\phi_r^{k\,(s+1)}$ are directly used as source terms for $\phi_b^{k\,(s+1)}$:

$$\left|\phi_r^k\right\rangle^{(s+1)} = -\mathbf{D}_r^{-1}(\mathbf{N}_b+\mathbf{M}_b)\cdot\left|\phi_b^k\right\rangle^{(s)} + S_r^{(n-1)},$$
$$\left|\phi_b^k\right\rangle^{(s+1)} = -\mathbf{D}_b^{-1}(\mathbf{N}_r+\mathbf{M}_r)\cdot\left|\phi_r^k\right\rangle^{(s+1)} + S_b^{(n-1)}. \qquad (11)$$

Convergence is brought by FDM, which gives spectral radii of iterative matrices of Eq.s (11) less than 1. Generally the finer the grid is, fewer discretization errors are introduced but the slower the CBS-Jacobi convergence might be found. In Eq.s (11), the Chebyshev's acceleration is applied as a successive over-relaxation method.

For a well-posed problem, suitable boundary conditions must be provided too. When reflected boundaries are met, it is:

$$J_i\big|_{bnd} = 0,\ J_i\big|_{bnd}\,\alpha\nabla_{\mathbf{r}}\phi(E)\big|_{bnd}\cdot\hat{e}_i \cong \delta(\Delta i^k)\left[\phi^k(E)-\phi(E)\big|_{bnd}\right]. \qquad (12)$$

Because the flux at the boundary is not calculated, like in any other position beyond, to allow all of its possible determinations δ is imposed to be vanishing. At first order, $D_i|_{bnd} \cong D_i^k$. The projection over energy groups, in the MGM, brings to null coefficients δ_g^k for ϕ_g^k too. For the MMM, the l-th weighting yields (see Eq. (10)):

$$J_{i,l}\big|_{bnd} = -\sum_{m=1}^{M} D_{lm}^{k} \frac{\partial a_m}{\partial i}\bigg|_{bnd} \cong$$
$$\sum_{m=1}^{M} \delta_{lm}(\Delta i^k)\left[a_m^k - a_m^{bnd}\right] = 0 \;\rightarrow\; \delta_{lm} = 0, \forall l,m \;. \tag{13}$$

In case zero flux is requested at the boundary, it comes that:

$$\phi\big|_{bnd} = 0\,,\; J_i\big|_{bnd} \cong \frac{2D(E)\big|_{bnd}}{\Delta i^k}\phi^k(E)\,. \tag{14}$$

For the MGM it is simply:

$$\phi_g\big|_{bnd} = 0\,,\; J_{i,g}\big|_{bnd} \cong \frac{2D_g^k}{\Delta i^k}\phi_g^k\,, \tag{15}$$

whereas for the MMM, a_m^{bnd} are all vanishing on the boundary:

$$\int_0^\infty U_l(E)\phi(E)\big|_{bnd}dE = \phi_l\big|_{bnd} =$$
$$\sum_{m=1}^{M} Q_{lm}a_m^{bnd} = \mathbf{Q}\cdot\left|a_m^{bnd}\right\rangle; \tag{16}$$
$$a_m^{bnd} = 0\,,\; J_{i,l}\big|_{bnd} \cong \sum_{m=1}^{M}\frac{2D_{lm}^k}{\Delta i^k}a_m^k\,.$$

In fact, in Eq. (16) the matrix **Q** is not singular.

In case of zero incoming current boundary condition, proportionality between the scalar flux and the current is expected at the boundary. Using again the finite difference form for the current, it turns out that the linearized flux goes to zero in a particular distance, properly called the extrapolated distance $d(E)$. Respectively for right and left core boundaries, it comes:

$$\phi\big|_{bnd} \mp \varsigma J\big|_{bnd} = 0\,,$$
$$\rightarrow \frac{\phi(E)\big|_{bnd}}{\varsigma D(E)} \cong \frac{\Delta\phi}{\Delta i} = \frac{\phi(E)\big|_{bnd} - 0}{d(E)}\,. \tag{17}$$

The coefficient ζ is chosen to be 2.13, using the transport relation $d = 0.71\,\lambda_{tr}$, with $D = \lambda_{tr}/3$ [11]. This value is close to the Marshak condition ($\zeta = 2$), for which the incoming current evaluated with the P_1 flux is null at the boundary. With different ζ, albedo conditions can also be selected. For the MGM, it becomes:

$$J_{i,g}\big|_{bnd} \cong \pm\frac{2D_g^k/\Delta i^k}{1+\varsigma(2D_g^k/\Delta i^k)}\phi_g^k\,. \tag{18}$$

For the MMM the extrapolation distance cannot have an easy treatment as it happens in Eq. (18). The projection of Eq. (17) on the l-th test function yields:

$$\sum_{m=1}^{M} a_m^{bnd}Q_{lm}^k = \sum_{m=1}^{M}(\mp\varsigma)D_{lm}^k\frac{\partial a_m}{\partial i}\bigg|_{bnd},$$
$$J_{i,j}\big|_{bnd} \cong \pm\sum_{m=1}^{M}\frac{2D_{lm}^k/\Delta i^k}{1+2d_{\mathrm{M}}/\Delta i^k}a_m^k\,. \tag{19}$$

Generally, in Eq. (19) an l-th and m-th extrapolation length $d_{\mathrm{M},lm}$ could be expected, but then undetermined problems arise. The simple choice $d_{\mathrm{M},lm} = \zeta\, D_{lm}^k / Q_{lm}^k$ does not return reliable physical results. A unique d_{M} implies the vanishing of the flux together with its migration modes over the same length. Eq. (19) in matrix notation and after some arrangements allows computing d_{M} by an eigenvalue problem:

$$\mathbf{R}_{lm}^k\cdot\left|a_m^{bnd}\right\rangle = d_M^{-1}\left|a_m^{bnd}\right\rangle,$$
$$\text{with } \mathbf{R}_{lm}^k = \varsigma^{-1}[\mathbf{D}_{lm}^k]^{-1}\mathbf{Q}_{lm}^k\,. \tag{20}$$

In Eq. (20), the physical eigenvalue corresponds to the spectral radius of $\{1/d_{\mathrm{M}}\}$, avoiding any possible negative values for migration modes. The hypothesis of the only dependence from the m-th single mode for d_{M}, like $d_{\mathrm{M}m}$, undergoes in a restriction which cannot be always verified, so rejected:

$$\mathbf{R}_{lm}^k\cdot\left|a_m^{bnd}\right\rangle = [\left\{d_m^{-1}\delta_{im}\right\}\mathbf{I}_{\mathbf{MxM}}]\cdot\left|a_m^{bnd}\right\rangle.$$

B. Second Level Solver with Nodal Expansions on Surfaces

Finite differences on a coarse mesh introduce strong discretization errors, which are refined by a Nodal Expansion Method (NEM). NEM starts after the completion of a PIM cycle. To save computation time, convergence criterion for PIM is relaxed not being reliable FDM required at the beginning of the numerical scheme. NEM corrects average nodal fluxes matching diffusion currents at all node interfaces. Consequently, two neighboring node problems are solved to estimate with higher accuracy surface flux and currents. Counting N nodes in the system, totally a set of 6 x N problems are expected to be solved. Continuity reduces them to 3 x N. The difference between each k-th NEM and CFDM currents for the i-th coordinate, $\delta J_i^{k\pm} = J_{i,NEM}^{k\pm} - J_{i,FDM}^{k\pm}$, provides corrections $\delta D_i^{k\pm}$ to diffusion coefficients. Its definition is not unique, but it must be consistent with the implementation in the CFDM. An equivalent form of Eq. (8) is chosen and for the MMM, it is:

$$\delta J_{i,l}^{k\pm} = \sum_{m=1}^{M}\delta J_{i,lm}^{k\pm} \cong$$
$$-\sum_{m=1}^{M}\delta D_{i,lm}^{k\pm}\frac{a_m^{k\pm1} + a_m^k}{(\Delta i^{k\pm1} + \Delta i^k)/2}\,. \tag{21}$$

In the MGM $\delta D_{i,g}^{k\pm}$ comes straightforwardly. In Eq. (21) the sum of mode coefficients is needed to avoid singular

behavior switching from currents to diffusion coefficient corrections. For reflected boundary conditions, $\delta J_i^{k\pm}$ are always vanishing on the contour. For all other boundary conditions, definitions of $\delta J_i^{k\pm}$ are:

$$\delta J_{i,g}^{k\pm} \cong -\delta D_{i,g}^{k\pm} \frac{\phi_{i,g}^k}{\Delta i^k / 2}\,,$$
$$\delta J_{i,l}^{k\pm} \cong -\sum_{m=1}^{M} \delta D_{i,lm}^{k\pm} \frac{a_m^k}{\Delta i^k / 2}\,. \tag{22}$$

In case a zero incoming current boundary occurs Eq. (22) is still assumed because simpler then Eq. (18) and Eq. (19).

After the NEM action, Eq. (7) is solved again by PIM, with new terms in the streaming operator:

$$\frac{1}{V^k}\iint_{S^k} \mathbf{J}(\mathbf{r},E)\cdot\hat{\mathbf{n}}\,dA = \sum_i \frac{J_{i,FDM}^{k+} + \delta J_i^{k+} - J_{i,FDM}^{k-} - \delta J_i^{k-}}{\Delta i^k}(E)\,. \tag{23}$$

Convergence for NEM cycles checks reaction rates and fluxes on all surfaces of nodes. In problems with external sources, NEM still keeps the outer level of iteration.

The node problem is based on the Transverse Integrated Procedure (TIP) reducing the dependence of the flux to a single variable [4]. TIP integrates the multi-dimensional diffusion equation, Eq. (7), over transverse directions to each coordinate axis. Then the transverse integrated flux is expanded with trial polynomial functions P_l (see App. A). By means of TIP, equations for the x direction follow; y and z directions are similarly treated. In the MMM and in the MGM, it becomes respectively:

$$a_m^k(x) = \sum_{l=0}^{R} \alpha_{m,l}^k P_l(x) \text{ and}$$
$$\phi_g^k(x) = \sum_{l=0}^{R} \alpha_{g,l}^k P_l(x)\,. \tag{24}$$

From Eq. (5), MMM cross sections are grouped under a unique term $\Sigma_{T,lm}^k$:

$$\Sigma_{T,lm}^k = \Sigma_{a,lm}^k + \Sigma_{r,lm}^k - \Sigma_{s,lm}^k - \chi_l^k \nu\Sigma_{f,m}^k / k_{eff} \tag{25}$$

For the MMM, TIP on Eq. (7) along the x direction for the k-th node yields:

$$\sum_{m=1}^{M}\left[-D_{lm}^k \frac{d^2}{dx^2} a_m^k(x) + \Sigma_{T,lm}^k a_m^k(x)\right] = \sum_{m=1}^{M} D_{lm}^k \left[\frac{L_{my}^k}{\Delta y^k} + \frac{L_{mz}^k}{\Delta z^k}\right], \text{ with } a_m^k(x) = \frac{1}{\Delta y^k \Delta z^k}\int_{\bar{y}^k-\Delta y^k/2}^{\bar{y}^k+\Delta y^k/2} dy \int_{\bar{z}^k-\Delta z^k/2}^{\bar{z}^k+\Delta z^k/2} dz\, a_m(\mathbf{r})\,. \tag{26}$$

For the MGM instead, it is:

$$-D_g^k \frac{d^2}{dx^2}\phi_g^k(x) + \Sigma_{t,g}^k \phi_g^k(x) - \sum_{g'=1}^{G}\left[\Sigma_{s,g'\to g}^k + \frac{\chi_g^k}{k_{eff}}\nu\Sigma_{f,g'}^k\right]\phi_g^k(x) = D_g^k\left[\frac{L_{gy}^k}{\Delta y^k} + \frac{L_{gz}^k}{\Delta z^k}\right], \text{ with } \phi_g^k(x) = \frac{1}{\Delta y^k \Delta z^k}\int_{\bar{y}^k-\Delta y^k/2}^{\bar{y}^k+\Delta y^k/2} dy \int_{\bar{z}^k-\Delta z^k/2}^{\bar{z}^k+\Delta z^k/2} dz\, \phi_g(\mathbf{r})\,. \tag{27}$$

In Eq. (26) and Eq. (27), $L_{m,j}^k$ and $L_{g,j}^k$ represents the m-th and g-th *transverse leakage* sink terms on the j-th coordinate ($j = \{y, z\}$):

$$\frac{L_{m,j}^k}{\Delta j^k} \cong \frac{1}{\Delta j^k}\left[\frac{\partial}{\partial j} a_m^k(x,j)\right]_{\bar{j}^k-\Delta j^k/2}^{\bar{j}^k+\Delta j^k/2},$$
$$\frac{L_{g,j}^k}{\Delta j^k} \cong \frac{1}{\Delta j^k}\left[\frac{\partial}{\partial j} \phi_g^k(x,j)\right]_{\bar{j}^k-\Delta j^k/2}^{\bar{j}^k+\Delta j^k/2}. \tag{28}$$

A scaling to the local reference frame is suitable to study directional flux inside the k-th node (see Fig. 2):

$$u = (x - \bar{x}^k)/\Delta x^k\,, \quad du = \Delta x^k dx\,. \tag{29}$$

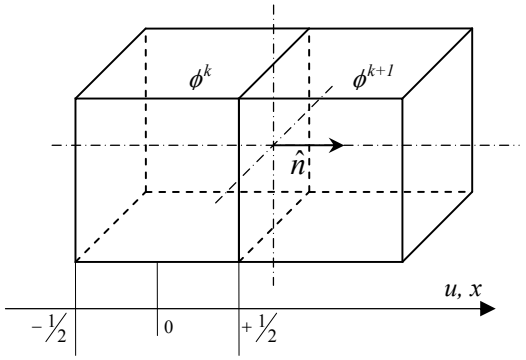

Fig. 2. Local reference frame for two node problem.

Using Eq.s (29) and substituting Eq. (24) into Eq. (26) and Eq. (27), Λ equations in Λ x (R + 1) unknowns come where Λ is respectively equal to M and G. A peculiar property of the expansion set is showing a P_0 orthogonal to all other P_l. It follows that $\alpha_{m,0}^k$ and $\alpha_{g,0}^k$ of the k-th node are assumed equal to the average m-th mode coefficient a_m^k and to the g-th flux ϕ_g^k, previously determined at the CFDM level. Fixing a fourth order polynomial treatment (R = 4) for both nodes, eight

equations for eight unknowns are requested. They are the continuity of the currents at interfaces, the continuity of the surface scalar flux and the last six relations are built with the application of the Weighted Residual technique (WR). WR is applied weighting over the first three expansion polynomials: P_0, P_1 and P_2. Again, being P_0 a constant, its weighting yields the net transfer leakage equation, *WR0*. For the MMM, it is:

$$\sum_{m=1}^{M}\left[2\frac{D_{lm}^{k}}{(\Delta x^{k})^{2}}\alpha_{m,2}^{k}+\frac{2}{5}\frac{D_{lm}^{k}}{(\Delta x^{k})^{2}}\alpha_{m,4}^{k}\right]= \sum_{m=1}^{M}\left[\frac{J_{lm,y}^{k+}-J_{lm,y}^{k-}}{\Delta y^{k}}+\frac{J_{lm,z}^{k+}-J_{lm,z}^{k-}}{\Delta z^{k}}+\Sigma_{T,lm}^{k}\alpha_{m,0}^{k}\right]. \quad (30)$$

MGM form is:

$$2\frac{D_{g}^{k}}{(\Delta x^{k})^{2}}\alpha_{g,2}^{k}+\frac{2}{5}\frac{D_{g}^{k}}{(\Delta x^{k})^{2}}\alpha_{g,4}^{k}= \frac{J_{g,y}^{k+}-J_{g,y}^{k-}}{\Delta y^{k}}+\frac{J_{g,z}^{k+}-J_{g,z}^{k-}}{\Delta z^{k}}+\Sigma_{t,g}^{k}\alpha_{g,0}^{k} -\sum_{g'=1}^{G}\left[\Sigma_{s,g'\to g}^{k}+\frac{\chi_{g}^{k}}{k_{eff}}\nu\Sigma_{f,g'}^{k}\right]\alpha_{g',0}^{k}. \quad (31)$$

Weighting over P_1, the MMM *WR1* comes:

$$\sum_{m=1}^{M}\left[\frac{1}{12}\Sigma_{T,lm}^{k}\alpha_{m,1}^{k}-\frac{1}{2}\left(\frac{D_{lm}^{k}}{(\Delta x^{k})^{2}}+\frac{1}{60}\Sigma_{T,lm}^{k}\right)\alpha_{m,3}^{k}\right] =\sum_{m=1}^{M}D_{lm}^{k}\left[\frac{1}{\Delta y^{k}}\int_{1/2}^{1/2}P_{1}L_{my}^{k}du+\frac{1}{\Delta z^{k}}\int_{1/2}^{1/2}P_{1}L_{mz}^{k}du\right], \quad (32)$$

while the MGM *WR1* is:

$$-\frac{1}{2}\left(\frac{D_{g}^{k}}{(\Delta x^{k})^{2}}+\frac{1}{60}\Sigma_{t,g}^{k}\right)\alpha_{g,3}^{k}+\frac{1}{12}\left\{\Sigma_{t,g}^{k}\alpha_{g,1}^{k} -\sum_{g'=1}^{G}\left[\Sigma_{s,g'\to g}^{k}+\frac{\chi_{g}^{k}}{k_{eff}}\nu\Sigma_{f,g'}^{k}\right]\cdot\left[\alpha_{g',1}^{k}-\frac{1}{10}\alpha_{g',3}^{k}\right]\right\} =D_{g}^{k}\left[\frac{1}{\Delta y^{k}}\int_{1/2}^{1/2}P_{1}L_{gy}^{k}du+\frac{1}{\Delta z^{k}}\int_{1/2}^{1/2}P_{1}L_{gz}^{k}du\right]. \quad (33)$$

For the MMM, *WR2* is:

$$\sum_{m=1}^{M}\left[\frac{1}{180}\Sigma_{T,lm}^{k}\alpha_{m,2}^{k} -\frac{1}{15}\left(\frac{D_{lm}^{k}}{(\Delta x^{k})^{2}}+\frac{1}{140}\Sigma_{T,lm}^{k}\right)\alpha_{m,4}^{k}\right]= \sum_{m=1}^{M}D_{lm}^{k}\left[\frac{1}{\Delta y^{k}}\int_{1/2}^{1/2}P_{2}L_{my}^{k}du+\frac{1}{\Delta z^{k}}\int_{1/2}^{1/2}P_{2}L_{mz}^{k}du\right], \quad (34)$$

and the MGM form is:

$$-\frac{1}{15}\left(\frac{D_{g}^{k}}{(\Delta x^{k})^{2}}+\frac{1}{140}\Sigma_{t,g}^{k}\right)\alpha_{g,4}^{k}+\frac{1}{180}\left\{\Sigma_{t,g}^{k}\alpha_{g,2}^{k} -\sum_{g'=1}^{G}\left[\Sigma_{s,g'\to g}^{k}+\frac{\chi_{g}^{k}}{k_{eff}}\nu\Sigma_{f,g'}^{k}\right]\cdot\left[\alpha_{g',2}^{k}-\frac{3}{35}\alpha_{g',4}^{k}\right]\right\} =D_{g}^{k}\left[\frac{1}{\Delta y^{k}}\int_{1/2}^{1/2}P_{2}L_{gy}^{k}du+\frac{1}{\Delta z^{k}}\int_{1/2}^{1/2}P_{2}L_{gz}^{k}du\right], \quad (35)$$

Continuity of l-th weighed currents at interface gives:

$$J_{l}^{k,+}=J_{l}^{k+1,-},\quad J_{l}^{k,\pm}=\lim_{u\to\pm1/2}J_{l}^{k}(u)= \sum_{m=1}^{M}-\frac{D_{lm}^{k}}{\Delta x^{k}}\left[\alpha_{m,1}^{k}\pm\alpha_{m,2}^{k}+\frac{1}{2}\alpha_{m,3}^{k}\pm\frac{1}{5}\alpha_{m,4}^{k}\right]; \quad (36)$$

while the correspondent equation for g-th currents yields:

$$J_{g}^{k,+}=J_{g}^{k+1,-},\quad J_{g}^{k,\pm}=\lim_{u\to\pm1/2}J_{g}^{k}(u)= -\frac{D_{g}^{k}}{\Delta x^{k}}\left[\alpha_{g,1}^{k}\pm\alpha_{g,2}^{k}+\frac{1}{2}\alpha_{g,3}^{k}\pm\frac{1}{5}\alpha_{g,4}^{k}\right]. \quad (37)$$

Each node represents generally a portion of fuel assembly and is filled with homogenized material data, disregarding any heterogeneity inside. The straight continuity of the flux would bring to results too far from more detailed reference calculation with neutron transport, considering all real heterogeneous effects indeed. Noticing the true flux at (±) interface as $\phi_{het}^{k,\pm}$ and with $\phi_{hom}^{k,\pm}$ the calculated one with homogenized cross sections, special coefficients $F^{k,\pm}(E) = \phi_{het}^{k,\pm}(E) / \phi_{hom}^{k,\pm}(E)$ act as discontinuity factors getting more reliable results at interfaces. Then, the continuity for the heterogeneous flux follows. Discontinuity factors $F_{lm,u}^{k,\pm}$ are evaluated as:

$$F_{lm,u}^{k,\pm}=\int_{0}^{\infty}dEU_{l}(E)\frac{\phi_{het}^{k}(E)}{\phi_{hom}^{k}(E)}Q_{m}(E). \quad (38)$$

Eq. (33) can also be written in an averaged sense as:

$$F_{lm,u}^{k,\pm}=F_{l,u}^{k,\pm}\cdot Q_{lm}, \text{ with}$$

$$F_{l,u}^{k,\pm}=\frac{\int_{0}^{\infty}dEU_{l}(E)\phi_{het}^{k}(E)}{\int_{0}^{\infty}dEU_{l}(E)\phi_{hom}^{k}(E)} \text{ and} \quad (39)$$

$$Q_{lm} = \int_0^\infty dE U_l(E) Q_m(E).$$

For both Eq. (33) and Eq. (34) $m = \{1, \ldots, M\}$. In the MGM, these coefficients comes simply integrating the continuity equation for ${\phi_{het}}^k$ on the g-th group, ${F_g}^{k,\pm} = {\phi_{het,g}}^{k,\pm} / {\phi_{hom,g}}^{k,\pm}$. ${\phi_{het}}^{k,\pm}$ must be provided through other more detailed calculations with cross section processing. Each l-th m-th discontinuity factor ${F_{lm,u}}^{k,\pm}$ is then applied to the correspondent m-th mode coefficient ${a_m}^k$ in the l-th equation:

$$\sum_{m=1}^{M} F_{lm,u}^{k,+} a_m^{k,+} = \sum_{m=1}^{M} F_{lm,u}^{k+1,-} a_m^{k+1,-},$$
$$a_m^{k,\pm} = \lim_{u \to \pm 1/2} a_m^k(u) = \alpha_{m,0}^k \pm \frac{1}{2}\alpha_{m,1}^k + \frac{1}{6}\alpha_{m,2}^k. \quad (40)$$

For the MGM, it is instead:

$$F_{g,u}^{k,+} \phi_g^{k,+} = F_{g,u}^{k+1,-} \phi_g^{k+1,-},$$
$$\phi_g^{k,\pm} = \lim_{u \to \pm 1/2} \phi_g^k(u) = \alpha_{g,0}^k \pm \frac{1}{2}\alpha_{g,1}^k + \frac{1}{6}\alpha_{g,2}^k. \quad (41)$$

Eq. (30), Eq. (32), Eq. (34), Eq. (36) and Eq. (40) state for with $l = \{0, \ldots, M-1\}$, while Eq. (31), Eq. (33), Eq. (35), Eq. (37) and Eq. (41) for with $g = \{1, \ldots, G\}$. Together with their similar forms of *WR0*, *WR1* and *WR2* for the $(k+1)$-th node, they constitute two closed inhomogeneous systems of linear equations, similarly solvable.

In case ${F_{lm,u}}^{k,\pm}$ could not be available through Eq. (38), the continuity for ${\phi_{het}}^k$ in the MMM can be formulated starting from Eq. (41), introducing ${F_{gm,u}}^{k,\pm} = {F_{g,u}}^{k,\pm} \cdot Q_{gm}$ after having developed ${\phi_g}^k$ with the MMM modal expansion. Q_{gm} is the projection of $Q_m(E)$ on the g-th group. The following relation is valid only for $G \le M$. The continuity for the heterogeneous flux in the MMM makes the approximation of disregarding the complementary part for the unknown synthesis error.

Boundary conditions must be satisfied by NEM too. Special node-boundary problems are needed for the only k-th node counting *WR0*, *WR1*, *WR2* equations and a closure for the boundary flux or current, specified by the proper condition. Zero current on a (±) surface is modeled by the MMM and the MGM respectively as:

$$\sum_{m=1}^{M} D_{lm}^k \left[\alpha_{m,1}^k \pm \alpha_{m,2}^k + \frac{1}{2}\alpha_{m,3}^k \pm \frac{1}{4}\alpha_{m,4}^k \right] = 0,$$
$$\alpha_{g,1}^k \pm \alpha_{g,2}^k + \frac{1}{2}\alpha_{g,3}^k \pm \frac{1}{4}\alpha_{g,4}^k = 0 \quad (42)$$

Zero flux boundary conditions are considered, again respectively for the MMM and the MGM, as:

$$\lim_{u \to \pm 1/2} \sum_{m=1}^{M} a_m^k(u) Q_{lm} =$$
$$\sum_{m=1}^{M} \left[\alpha_{m,0}^k \pm \frac{1}{2}\alpha_{m,1}^k + \frac{1}{6}\alpha_{m,2}^k \right] Q_{lm} = 0,$$
$$\lim_{u \to \pm 1/2} \phi_g^k(u) =$$
$$\alpha_{g,0}^k \pm \frac{1}{2}\alpha_{g,1}^k + \frac{1}{6}\alpha_{g,2}^k = 0. \quad (43)$$

About the zero incoming current boundary condition, TIP brought upon Eq. (17) gives:

$$\lim_{u \to \pm 1/2} \left[\phi^k(u,E) \pm \varsigma \frac{D^k(E)}{\Delta x^k} \frac{\partial}{\partial u} \phi^k(u,E) \right] = 0. \quad (44)$$

Introducing l-th weighting of MMM, Eq. (44) is modified as:

$$\lim_{u \to \pm 1/2} \sum_{m=1}^{M} \left[a_m^k(u) Q_{lm} \pm \varsigma \frac{D_{lm}^k}{\Delta x^k} \frac{d}{du} a_m^k(u) \right] =$$
$$\sum_{m=1}^{M} \left[\left(\pm \alpha_{m,0}^k + \frac{1}{2}\alpha_{m,1}^k \pm \frac{1}{6}\alpha_{m,2}^k \right) Q_{lm} \right.$$
$$\left. + \varsigma \frac{D_{lm}^k}{\Delta x^k} \left(\alpha_{m,1}^k \pm \alpha_{m,2}^k + \frac{1}{2}\alpha_{m,3}^k \pm \frac{1}{5}\alpha_{m,4}^k \right) \right] = 0; \quad (45)$$

while in MGM, it is:

$$\pm \alpha_{g,0}^k + \frac{1}{2}\alpha_{g,1}^k \pm \frac{1}{6}\alpha_{g,2}^k$$
$$+ \varsigma \frac{D_g^k}{\Delta x^k} \left[\alpha_{g,1}^k \pm \alpha_{g,2}^k + \frac{1}{2}\alpha_{g,3}^k \pm \frac{1}{5}\alpha_{g,4}^k \right] = 0. \quad (46)$$

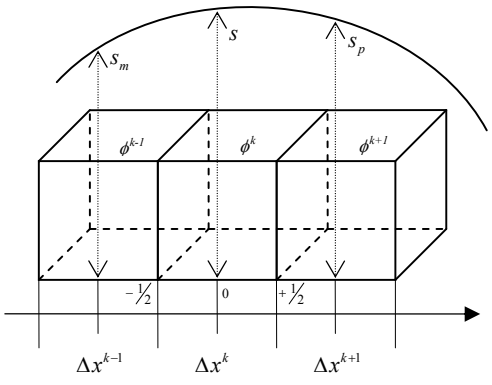

Fig. 3. Quadratic transverse leakage scheme.

C. Transverse Leakage

In *WR0*, *WR1* and *WR2* quadratures of transverse leakage terms, introduced by TIP, appear needing a proper treatment. In this section, the discussion concerns the *x* coordinate. The extension to the other ones is straightforward. MMM form is plainly presented, but MGM does not show any theoretical difference. The transverse leakage, here called S_{tr}, is approximated polynomially at the second order along the local coordinate *u* as:

$$S_{tr} = D_{lm}^{k}\left[\frac{L_{my}^{k}}{\Delta y^{k}} + \frac{L_{mz}^{k}}{\Delta z^{k}}\right], \quad S_{tr} = a + bu + cu^{2}. \qquad (47)$$

a, *b* and *c* in Eq. (47) are determined through (see Fig. 3):

$$\begin{cases} \int_{-1/2-\Delta x^{k-1}/\Delta x^{k}}^{-1/2} S_{tr}(u)du = s_m, \\ \int_{-1/2}^{1/2} S_{tr}(u)du = s, \\ \int_{1/2}^{1/2+\Delta x^{k+1}/\Delta x^{k}} S_{tr}(u)du = s_p. \end{cases} \qquad (48)$$

In case of an equally spaced grid, $\Delta x^{k-1} = \Delta x^{k} = \Delta x^{k+1}\ \forall k$, it is simply:

$$a = \frac{13}{12}s - \frac{s_p + s_m}{24},\ b = \frac{s_p - s_m}{2},\ \text{and}\ c = \frac{s_p + s_m}{2} - s. \qquad (49)$$

Weighted integrals with WR of the transverse leakage, in Eq. (32) and Eq. (34) for the MMM, in Eq. (33) and Eq. (35) for the MGM, simply become (see App. A):

$$WR1: \int_{-1/2}^{1/2} P_1(u)S_{tr}(u)\,du = \frac{b}{12}, \qquad WR2: \int_{-1/2}^{1/2} P_2(u)S_{tr}(u)\,du = \frac{c}{180}. \qquad (50)$$

VI. Results

A simple nuclear core is studied by the presented diffusion model with two group (2G) MGM and the correspondent two mode (2M) MMM to verify the coded schemes. 2M MMM takes Q_M and a coupling between χ and Q_{SD} as migration modes. 2G MGM calculations are commonly used in standard industrial codes. Solutions of a 99G MGM bring reference results. Used material constants of each node are homogenized and collapsed starting from the same reference 99G data libraries following Eq.s (4) and Eq.s (5). Lateral surfaces, arranged in square corners, describe neighboring assemblies as shown in Fig. 4, in a matrix of 210 x 210 x 220 cm. The core is fully loaded with PWR 17 x 17 UO_2 fuel assemblies enriched at 3.5 % in ^{235}U. Cross sections are produced at Hot Zero Power: moderating water temperature of 310 °C and density of 0.7 g/cm^3, diluted boron atomic density of $1.665 \cdot 10^{-5}$ g-atom/barn/cm. An attempt with an external water reflector has also been considered, making some assumptions on the correspondent collapsing spectrum. When no reflector is considered, fuel elements take its place. Dirichlet zero flux conditions are simply assumed all over the core boundaries.

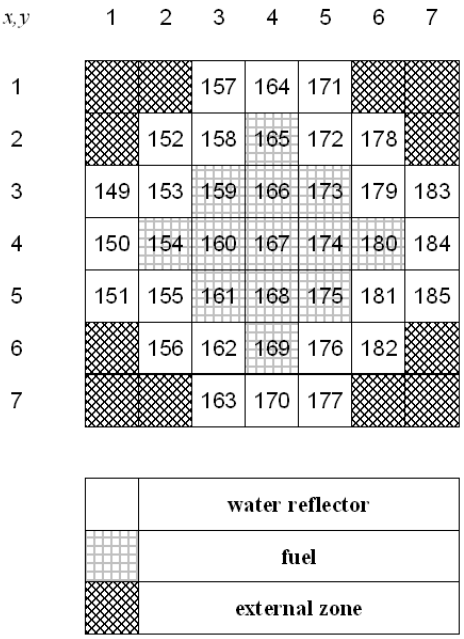

Fig. 4. Core Layout with node indexing at 5-th z level (max level equal to 8)

For the processing of MMM material constants, the classical adjoint spectrum and the generalized adjoint one, referring to the spectral index as observable parameter, have been employed in each test function set.

Being the neutron slowing down the hardest phenomenon to describe, different forms for the mode Q_{SD} have been conceived to investigate its effects in the whole system. These listed *i*-th options MMM(*i*) offer different Q_{SD} computed by:

1. the cross section dependent Gandini's formula [8];
2. Dall'Osso's formula [7];
3. heuristically, making the difference between the Maxwellian and reference spectrum;
4. Dall'Osso's formula with fitting of exponents by the ordinary least square technique, featuring the resonance self-shielding.

Still, *i*.2 refers to an optimization algorithm acting on the coupling between χ and Q_{SD} to match the reference spectral index. k_{eff} results without any reflector follow in Tab. I.

TABLE I
RESULTS OF k_{eff} IN ABSENCE OF EXTERNAL REFLECTOR.

	k_{eff} - FDM -	k_{eff} - NEM -	Δk (pcm)	
			(FDM - *Ref*)	(NEM - *Ref*)
99G	**1.032036**	**1.030532**	**150.4**	**0.0**
2G	1.032719	1.031401	218.7	86.9
MMM1	1.031268	1.029917	73.6	-61.5
MMM1.2	1.033175	1.031874	264.3	134.2
MMM2	1.028506	1.027077	-202.6	-345.5
MMM2.2	1.032352	1.031030	182.0	49.8
MMM3	1.032306	1.030980	177.4	44.8
MMM4	1.031723	1.030381	119.1	-15.1
MMM4.2	1.032678	1.031367	214.6	83.5

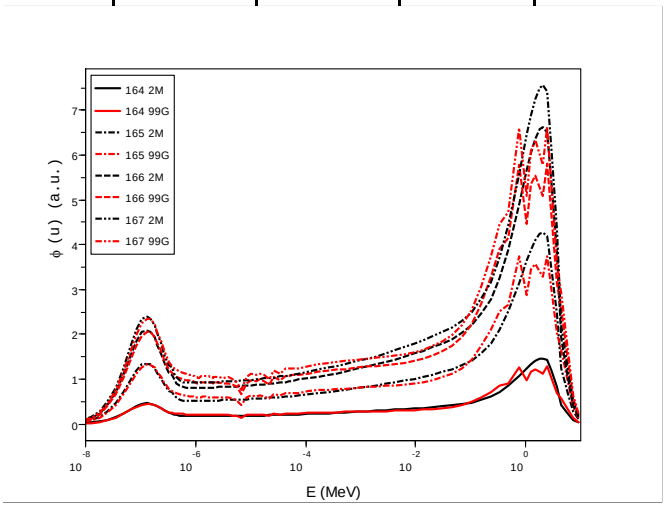

Fig. 5. Computed 2M and 99G spectra from the node 164 towards the central 167 (see Fig. 4).

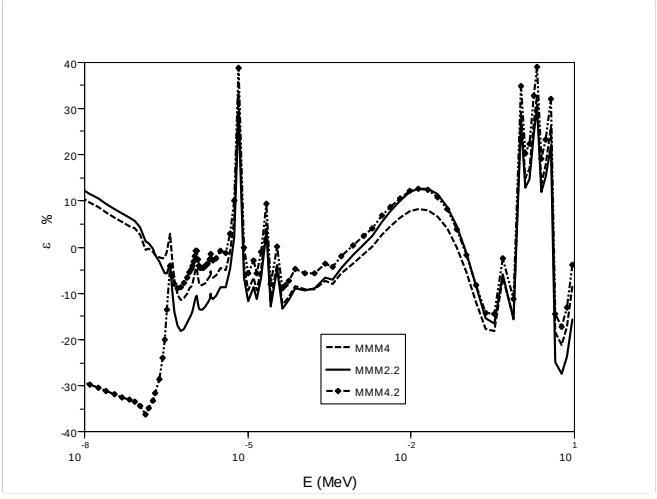

Fig. 6. Relative error between some computed 2M and 99G spectra along the axis of nodes 164 - 167.

For the fuel homogeneity, good results on the multiplicatively constant k_{eff} are achieved by options of MMM which compute accurately the reference spectrum of infinite medium, by which cross section processing was executed. Tab. I shows also the net improvements gained by NEM.

Fig. 5 plots evaluated spectra of MMM2.2 and 99G MGM for a radial portion of the core (see Fig. 4). For the same core loading, spectral differences are simply scaled node by node, from the center to the boundary. Fig. 6 draws the spectral error for MMM2.2, MMM4.2 and MMM4 towards 99G spectra.

Errors at thermal energies for MMM4.2, as confirmed in Tab. I, make thinking of unsuited best fitting. Although MMM4 behaves well in this example, other tests in heterogeneous media advices the adoption of MMM2.2 for standard Q_{SD} [14]. However it must be reminded that all these options come from MMM2. MMM1 has been disregarded in favor of MMM2 variants because of its too problem-dependent feature, which could need several material data generation during feedback calculations in typical industrial applications. Furthermore, because of analytical trial functions, MMM2 allows easier computation of migrating modes.

The agreement between MMM3 and MMM2.2 in Tab. I suggests the skill of MMM2.2 to predict averagely well the neutron phenomena at epithermal and high energies. The MMM3 k_{eff} error, by definition, estimates directly spectral leakage effects onto the criticality of the system.

Introducing the external reflector spectral changes can be better investigated. The reflector layer folds also bottom and upper z-levels of the core (see Fig. 4). Water filling this zone has the same properties of the cooling one, used for fuel assembly cross section processing. The choice of a proper collapsing spectrum for the reflector is critical in case of the 2G, while for the 2M, migration modes still keep their generality. Initially cross sections were collapsed by the infinite medium spectrum of the fuel material. Then, the 99G spectrum of the boundary node 22 (position of node 170 at z = 1 in Fig. 4) was used, obtaining more accurate 2G results then with spectra of lateral nodes.

Tab. II collects correspondent results for the k_{eff}. The first collapsing choice is here labeled with *a*, while the latter with *b*. MMM4 reconstructed fluxes appear in Fig. 7 evaluated in lethargy u with the collapsing spectrum coming from node 22. Fig. 8 shows instead the relative differences between the spectrum of the node 22 and the ones of nodes 170 (lateral sides, see Fig. 4) and 19 (bottom center at $x = y = 4$, $z = 0$), carefully chosen. Drawn fluxes consider a common normalization to underline different shapes. Tab. II confirms that the exact reconstruction of MMM3 for a good spectrum in the infinite medium isn't always a good marker for a likewise description in real 3D systems.

TABLE II
RESULTS OF k_{eff} WITH THE EXTERNAL REFLECTOR: REFLECTOR CROSS SECTION COLLAPSED WITH THE FUEL SPECTRUM (*a*) AND THE ONE OF NODE 22 (*b*).

	k_{eff} - FDM -	k_{eff} - NEM -	Δk (pcm)	
			(FDM - *Ref*)	(FDM - *Ref*)
99G	**1.010035**	**1.010102**	**-6.7**	**0.0**
2G.a	1.011737	1.012260	163.5	215.8
2G.b	1.011739	1.011019	163.7	91.7
MMM1.a	1.009314	1.009985	-78.8	-11.7
MMM1.2.a	1.012036	1.012580	193.4	247.8
MMM2.a	1.005260	1.006159	-484.2	-394.3
MMM2.2.a	1.010846	1.011471	74.4	136.9
MMM2.b	1.000950	1.005621	-915.2	-448.1
MMM2.2.b	1.006672	1.010997	-343.0	89.5
MMM3.a	1.011774	1.011368	167.2	126.6
MMM4.a	1.010254	1.010924	15.2	82.2
MMM4.b	1.006549	1.010482	-355.3	38.0

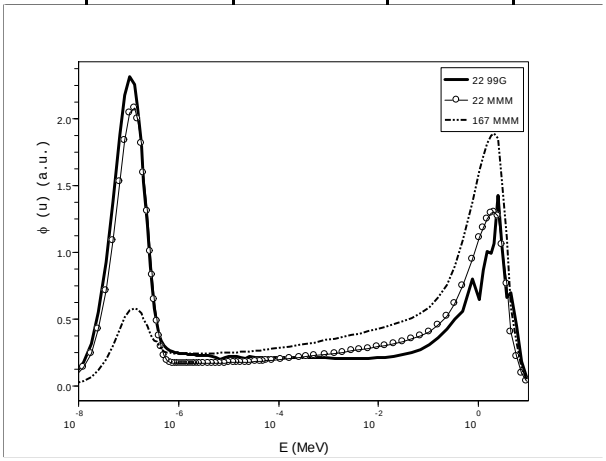

Fig. 7. Spectral differences of nodes 19 (bottom center) and 167 (core center) relative to the spectrum of node 22, used to collapse reflector cross sections.

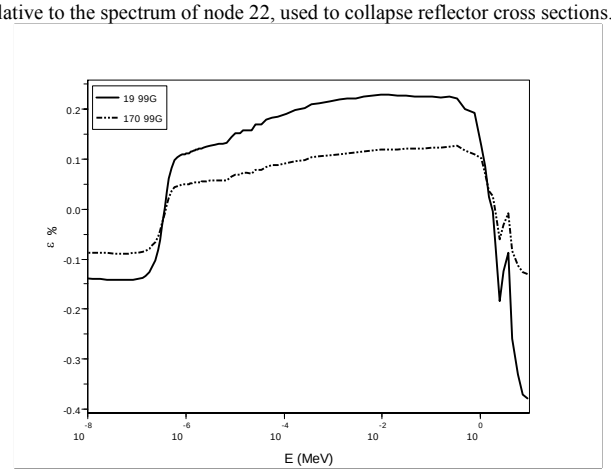

Fig. 8. Spectral differences of nodes 19 and 170 relative to the spectrum of node 22, used to collapse reflector cross sections.

MMM predict with good accuracy the reflector spectrum at thermal energies. Only derived MMM2 versions perform better at higher energies. MMM4 flux is plotted along the radial coordinate in Fig. 9, proposing successive node spectra from the center of the system (node 167) to the boundary (node 170). A scaled behavior is verified till reaching the reflector, where thermal neutrons gains importance against the fast pick.

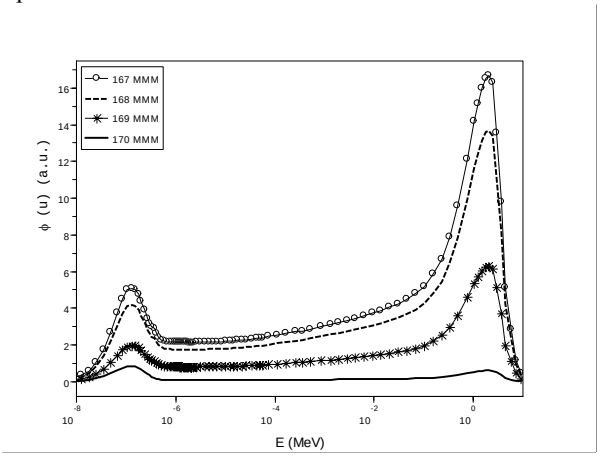

Fig. 9. Radial MMM4 spectra considering the water reflector (node 170).

VII. Appendix A

The polynomial function set adopted in this work for nodal expansions of NEM is, with $u \in [-1/2, +1/2]$ and $R = 4$:

$$\begin{aligned} P_0(u) &= 1 \ , \\ P_1(u) &= u \ , \\ P_2(u) &= u^2 - 1/12 \ , \\ P_3(u) &= u\,(u^2 - 1/4) \ , \\ P_4(u) &= (u^2 - 1/4)(u^2 - 1/20) \ ; \end{aligned} \tag{51}$$

with:

$$\int_{-1/2}^{1/2} P_i(u)du = \delta_{i0} \ ,$$

$$\int_{-1/2}^{1/2} P_i(u)P_j(u)du = \mathbf{C}_{i,j} \ , \quad \mathbf{C} = \{C_{ij}\} =$$

$$\begin{bmatrix} 1 & 0 & 0 & 0 & 0 \\ 0 & \frac{1}{12} & 0 & -\frac{1}{120} & 0 \\ 0 & 0 & \frac{1}{180} & 0 & -\frac{1}{2100} \\ 0 & -\frac{1}{120} & 0 & \frac{1}{840} & 0 \\ 0 & 0 & -\frac{1}{2100} & 0 & \frac{1}{15750} \end{bmatrix} , \tag{52}$$

being $i, j = \{0, 1, 2, 3, 4\}$.

Derivatives on polynomials yield:

$$\frac{d}{du}\cdot\mathbf{I}_{5X5}\cdot\begin{bmatrix}P_0\\P_1\\P_2\\P_3\\P_4\end{bmatrix}=\begin{bmatrix}0\\P_0\\2P_1\\3P_2\\4P_3+2/5P_1\end{bmatrix},$$

$$\frac{d^2}{du^2}\cdot\mathbf{I}_{5X5}\cdot\begin{bmatrix}P_0\\P_1\\P_2\\P_3\\P_4\end{bmatrix}=\begin{bmatrix}0\\0\\2P_0\\6P_1\\12P_2+2/5P_0\end{bmatrix}. \qquad (53)$$

VIII. Acknowledgment

The author expresses his grateful acknowledge to A. Dall'Osso (AREVA NP) for his important contribution in the MMM development and for the many useful advices in the preparation of the paper.

IX. Conclusions

The theory of a diffusion model for steady state calculations with the MMM has been successfully developed and implemented in a computer code, following a similar approach for the MGM. The coupling of FDM and NEM counting accelerations and symmetries performs quick calculations in few seconds. New features, typical of industrial computer codes, are going to be applied in order to simulate full real nuclear cores with thermal feedbacks. Test cases show sensitivity to the choice of the migration mode for the slowing-down, mainly due to self-shielding effects. The work has allowed achieving a better insight into the MMM, also with significant improvements for the theory. Comparisons between 2G MGM and 2M MMM, with respect to 99G MGM reference calculations, display interesting results for the detailed information kept by MMM in energy. MMM shows an intrinsic benefit following variations of the spectrum shape in the whole system. Further studies on migration modes are foreseen to improve the neutron spectrum description, considering also spatial leakage corrections. Once proper sets for migration modes have been provided, the MMM can make detailed syntheses of any nuclear core model, without suffering limitations for its application to a particular reactor type.

X. References

Periodicals:

[1] C. H. Westcott, "The specification of neutron flux and nuclear cross_sections in reactor calculations," *Journal of Nuclear Energy*, vol. 2, pp. 59-76, 1955.

[2] W. M. Stacey, "A general modal-expansion method for obtaining approximate equations for linear systems," *Nuclear Science and Engineering*, vol. 28, pp. 438-442, 1967.

[3] W. M. Stacey, "General Multigroup and Spectral Synthesis Equations," *Nuclear Science and Engineering*, vol. 40, pp. 73-90, 1970.

[4] R. D. Lawrence, "Progress in nodal methods for the solution of the neutron diffusion and transport equations," *Progress in Nuclear Energy*, vol. 17, No. 3, pp. 271-301, 1986.

[5] M. T. Vilhena, L. B. Barichello, J. R. Zabadal, C. F. Segatto, A. V. Cardona and R. P. Pazos, "Solutions to the multidimensional linear transport equation by the spectral method," *Progress in Nuclear Energy*, vol. 35, No. 3-4, pp. 275-291, 1999.

[6] B. Neta, S. Reich, H. D. Jr Victory, "Galerkin spectral synthesis methods for diffusion equations with general boundary conditions," *Annals of Nuclear Energy*, vol. 29, pp. 913-927, 2002.

[7] A. Dall'Osso, "Introducing the migration mode method for the solution of the space and energy dependent diffusion equation," *Annals of Nuclear Energy*, vol. 30, pp. 1829-1845, 2003.

[8] A. Dall'Osso, A. Gandini and R. Rotella, "Investigations on the migration mode method (MMM) for reactor calculations," *Annals of Nuclear Energy*, vol. 35, pp. 1306-1313, 2008.

[9] F. Rahnema, S. Douglass, B. Forget, "Generalized energy condensation theory," *Nuclear Science and Engineering*, vol. 160, pp. 41-58, 2008.

Books:

[10] B. Davison, Neutron Transport Theory, Oxford: Clarendon Press, 1957.

[11] J.R. Lamarsh, "Introduction to Nuclear Reactor Theory," Addison-Wesley, Reading, MA, 1966.

[12] G.I. Bell and S. Glasstone, "Nuclear Reactor Theory", New York: Van Nostrand Reinhold, 1970.

Papers from Conference Proceedings:

[13] I. K. Attieh, R. E. Pevey, "A new generalized multigroup method," Proceedings of the International Physor Conference (PHYSOR 2002), Seoul, Korea, October 7-10, 2002.

[14] D. Tomatis and A. Dall'Osso, "Improvement and core applications of the Migration Mode Method," International Conference on Mathematics, Computational Methods & Reactor Physics (M&C 2009), Saratoga Springs, New York, May 3-7, 2009.

XI. Biographies

Daniele Tomatis is a PhD candidate in Energetics at Politecnico di Torino, Italy, where he got bachelor and master degrees too, respectively in 2004 and 2006. His career counts several experiences of collaboration with the R&D of AREVA NP and the OPTIME award given in 2007 by the Unione Industriale di Torino. His current area of research is Reactor Physics for fission neutron multiplying systems with special attention to spectral synthesis methods and computer codes.